CMLS, Cell. Mol. Life Sci. 61 (2004) 763–773
1420-682X/04/080763-11
DOI 10.1007/s00018-003-3404-1

CMLS Cellular and Molecular Life Sciences

Subatomic and atomic crystallographic studies of aldose reductase: implications for inhibitor binding

A. Podjarny [a, *], R. E. Cachau [b], T. Schneider [c, f], M. Van Zandt [d] and A. Joachimiak [e]

[a] Laboratoire de Génomique et de Biologie Structurales, UMR 7104 du CNRS, IGBMC, 1 rue Laurent Fries, BP 163, 67404 Illkirch Cedex (France), e-mail: podjarny@titus.u-strasbg.fr
[b] Advanced Biomedical Computing Centre, National Cancer Institute, SAIC, Frederick, Maryland 21702 (USA)
[c] Göttingen University, Department of Structural Chemistry, Tammannstr. 4, 37077 Göttingen (Germany)
[d] Institute for Diabetes Discovery, Inc., Branford, Connecticut (USA)
[e] Structural Biology Center, Biosciences Division, Argonne National Laboratory, Argonne, Illinois (USA)
[f] Current address: FIRC Institute of Molecular Oncology, Via Adamello 16, 20139 Milan (Italy)

Abstract. The determination of several of aldose reductase-inhibitor complexes at subatomic resolution has revealed new structural details, including the specific interatomic contacts involved in inhibitor binding. In this article, we review the structures of the complexes of ALR2 with IDD 594 (resolution: 0.66 Å, IC50 (concentration of the inhibitor that produced half-maximal effect): 30 nM, space group: $P2_1$), IDD 393 (resolution: 0.90 Å, IC50: 6 nM, space group: P1), fidarestat (resolution: 0.92 Å, IC50: 9 nM, space group: $P2_1$) and minalrestat (resolution: 1.10 Å, IC50: 73 nM, space group: P1). The structures are compared and found to be highly reproductible within the same space group (root mean square (RMS) deviations: 0.15 ~ 0.3 Å). The mode of binding of the carboxylate inhibitors IDD 594 and IDD 393 is analysed. The binding of the carboxylate head can be accurately determined by the subatomic resolution structures, since both the protonation states and the positions of the atoms are very precisely known. The differences appear in the binding in the specificity pocket. The high-resolution structures explain the differences in IC50, which are confirmed both experimentally by mass spectrometry measures of VC50 and theoretically by free energy perturbation calculations. The binding of the cyclic imide inhibitors fidarestat and minalrestat is also described, focusing on the observation of a Cl^- ion which binds simultaneously with fidarestat. The presence of this anion, binding also to the active site residue His110, leads to a mechanism in which the inhibitor can bind in a neutral state and then become charged inside the active site pocket. This mechanism can explain the excellent in vivo properties of cyclic imide inhibitors. In summary, the complete and detailed information supplied by the subatomic resolution structures can explain the differences in binding energy of the different inhibitors.

Key words. Aldose reductase inhibition; subatomic resolution crystallography.

Introduction

The diffraction of X-rays by molecular crystals is the technique of reference for obtaining three-dimensional information about atomic positions and interactions, information essential for the comprehension of function and molecular mechanisms. In the case of small molecules, very precise high-resolution measurements allow the observation of hydrogen atoms and of bond electronic densities. Thus, relations could be established between the deviations from standard stereochemistry of spherical atomic models and chemical reactivity. In the case of biological macromolecules, one could correlate the spatial arrangement of the components of proteins and nucleic acids to their biological function.

These two types of studies progressed independently during the last 2 decades, primarily because of the limited resolution of the macromolecular crystallographic re-

* Corresponding author.

sults: 2–3 Å in the majority of cases, against 0.5 Å or better for small molecules. Resolution, which is the minimal separation of the crystal plans giving place to an observable X-ray diffraction spot, is indeed an essential parameter of a crystallographic study. It is directly related to the minimum distance separating the details of electronic density. A resolution of 2 Å is sufficient to distinguish peptides from a protein or the bases of a nucleic acid, but not the individual atoms, and even less the bond densities. In the last 10 years, various technical improvements, ranging from better techniques of expression and crystallisation to the use of synchrotron sources for measurements of diffraction and algorithms of multipolar and quantum modelling, made it possible to considerably improve the resolution and quality of macromolecular models [1]. Biological structural studies with resolutions between 1.5 and 0.9 Å became more current [2–3]. In this range of resolution, the individual atoms can be clearly distinguished, and the hydrogen atoms start to appear. As the uncertainities of atomic position are reduced by an order of magnitude (typically from 0.2 to 0.03 Å), the observed deviations from standard stereochemistry start to be significant.

Since 1997, several structures were solved with a resolution better than 0.9 Å, in particular crambin [4–5], subtilisin [6], and aldose reductase [7]. With such resolution, the level of the details observed in the best-ordered areas approaches that of small molecule studies. Hydrogen atoms and bond densities are clearly visible, and the atomic errors of coordinates are reduced by another order of magnitude (~ 0.003 Å), which makes the stereochemical differences highly significant [8–10]. Estimation of the atomic charges starts to be possible [5].

In the case of aldose reductase (AR), crystals of a complex with the inhibitor IDD594 diffracted up to 0.66 Å, the highest resolution observed so far for a protein of this size (35 KD). Furthermore, several structures of complexes with different inhibitors were determined to subatomic resolution, enabling comparison of the structural features and of the charge states. This leads to a deeper understanding of the mechanism of inhibitor binding, which is described below.

High resolution AR structures

Though several crystallographic structures have been solved for aldose reductase, the most remarkable results – to understand the inhibition mechanim from a methodological point of view – come from high and ultra-high-resolution crystallographic studies [11].

AR diffraction data at atomic and subatomic resolution have been collected and the structure have been solved for complexes with the following inhibitors:

1) IDD-594, 0.66 Å, carboxylate head, IC50: 30 nM [25]
2) IDD-393, 0.9 Å, carboxylate head, IC50: 6 nM [sent to publication]
3) SNK-860 (fidarestat), 0.9 Å, hydantoin head, IC50: 9 nM [12]
4) WAY-509 (minalrestat), 1.1 Å, hydantoin head, IC50: 73 nM [12]

The high-resolution structures of SNK-860 and WAY-509 [12] have been described in the previous review on AR – inhibitor structures. IDD-594 and IDD-393 are close to Ponalrestat (Statil), with the difference that the double-ring system is replaced by a single ring plus an internal hydrogen bond [13] (fig. 1).

Crystallization and structure solution

Human AR was expressed in *Eschericchia coli* and co-crystallised with the oxidised form of the coenzyme (β-$NADP^+$) with the different inhibitors at pH 5.0 and at 277 K, using ammonium citrate buffer and poly(ethylene glycol) (PEG) as the precipitating agent [14]. Two different space groups, P1 and $P2^1$, can be obtained with the same crystallisation conditions, as shown in table 1. The crystal diffraction quality was significantly improved by cocrystallisation with the cofactor and inhibitor, by microseeding and by optimisation of the cryofreezing protocol [7]. Diffraction experiments were conducted on the undulator line 19ID of Structural Biology Center Collaborative Access Team (SBC-CAT) at the Advanced Photon Source (APS) and on the Photon Source (PX) line at the

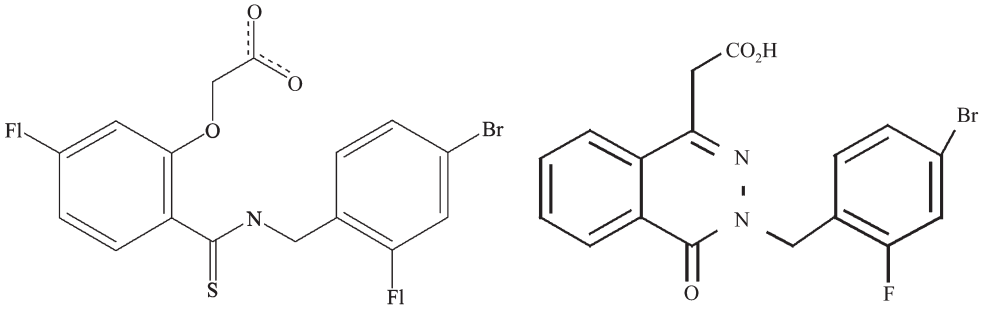

Figure 1. Scheme of IDD594 inhibitor structure vs. ponalrestat.

Table 1. Statistics of data collection and refinement.

Data collection	IDD 594	IDD 393	SNK 860	WAY 509
Resolution	20–0.66	50–1.0	99.0–0.92	50.0–1.1
Rmerge	0.029	0.062	0.036	0.041
I/s(I)	14.5	13.7	13.5	25.6
# reflections	511247	158045	193488	115145
space group	$P2^1$	P1	$P2^1$	$P2^1$
Cell dimensions				
a, b, c (Å)	49.43, 66.79, 47.40	47.2, 47.15, 40.31	49.4, 67.0, 47.3	40.0, 47.1, 47.4
α, β, γ (°)	90, 92.4, 90	67.58, 76.47, 76.11	90.0, 92.1, 90.0	75.7, 67.5, 76.8
Solvent content	34%	34.4%	34%	34.4%
Final model				
Residues	313	316	316	316
NADP	1	1	1	1
Inhibitor	1	1	1	1
Citrate	2	0	0	0
Water	613	428	597	427
Residues with non-unit occupancies	99	63	98	42
R-factor/Rfree (all reflections)	9.38/10.33%	11.04/13.33%	10.42/12.85	9.86/12.42

Swiss Light Source (SLS) [Sanishvilli et al., in preparation]. Several scans in different sample orientations and in four different resolution shells allowed the accumulation of sufficient completeness and redundancy to ensure accurate measurements [26]. The structures were solved using the molecular replacement method [15–16], and refined with CNS and SHELX [16].

The different structures are remarkably similar, as seen in table 2, which shows the RMS deviation difference between all CA atoms (top right) and CA atoms with $B < 5$ in the IDD 594 structure (bottom left). Note that the smallest differences (bold) are obtained between structures solved in the same space group.

Figure 2 shows the superposition of the different structures (594: yellow; 860: green; 509: red; 393: blue) which are essentially identical with the exception of the loops around the active site.

The inhibitors occupy the same place in the active site cleft. Three of them (594, 393 and 509) enter the specificity pocket (for definition of the specificity pocket, see the previous review by el-Kabbani et al. [13]), while the fourth one (860) does not.

Table 2. RMS differences between CA atoms in different complexes.

	IDD 594 (P21)	SNK 860 (P21)	IDD 393 (P1)	WAY 509(P1)
IDD 594 (P21)		**0.31**	0.51	0.45
SNK 860 (P21)	**0. 20**		0.55	0.50
IDD 393 (P1)	0.35	0.37		**0.23**
WAY 509 (P1)	0.30	0.33	**0.15**	

Carboxylate inhibitors: IDD 594 and IDD 393

The inhibitors IDD 594 and IDD 393 were prepared as part of a cogeneric family sharing a common scaffold (fig. 3). The structure-activity relations indicate that the carboxylate moiety, the ether oxygen of the phenoxyacetic acid and the amide N-H are necessary for activity. The carboxylate group appears to be particularly necessary for efficient inhibition. The aromatic side chain is critical for both potency and selectivity [M. Van Zandt et al., in preparation]. The observed selectivity pattern is consistent with the major differences between human AR 2 (hALR2) and 1 (hALR1), which are in the C-terminal loop (adjacent to the aromatic side chain) [17–18]. The preferred substitution pattern for the benzyl side chain is either a 6-nitro group (IDD 393), or a fluorine in the 5-position with a bromide in the 7-position (IDD 594). The affinity and selectivity of these inhibitors is pointed by the IC50 values against AR (= 30 nM, IDD 393 = 6 nM) vs. the ones against AR (IDD 594 = 33000 nM, IDD 393 = > 50000 nM).

The inhibitors bind similarly to the active site cleft and the specificity pocket [19] (fig. 4). The accuracy of the experimental data allows observation of individual electron densities for each atom (see fig. 5), deviations from the spherical atom model in an electron difference map, correlations between C-O and C-N bond lengths and some deviations of the ω angle in peptide bonds [20], unusually short distances CH-O, ordered solvent molecules and 54% of all the possible atoms in the protein. This last fact permits the unequivocal assignement of the protonation states in the active site zone (a well-ordered region with B-factors between 3 and 5 $Å^2$).

The protonation states were specially analysed for IDD 594. The difference electron density map contoured at

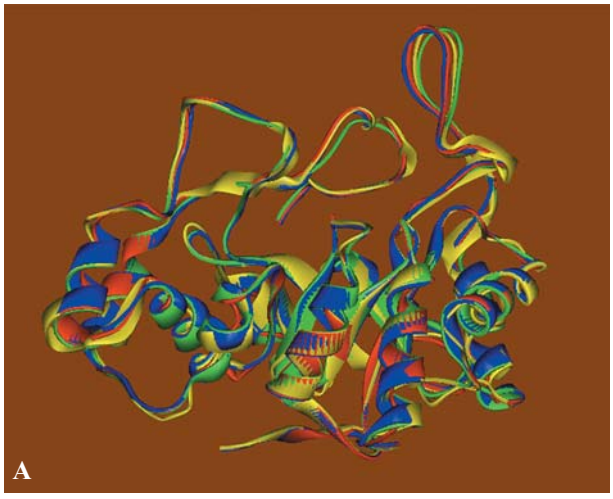

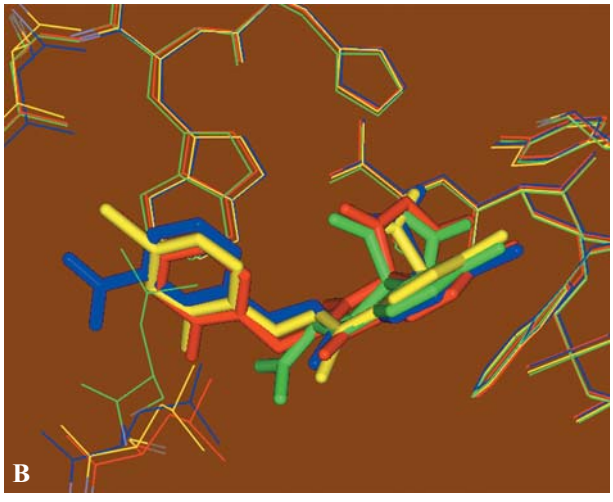

Figure 2A, B. (*a*) Superposition of the different structures (594: yellow; 860: green; 509: red; 393: blue) which are essentially identical with the exception of the loops around the active site. (*b*) Same as (*a*), zoomed on the inhibitor binding site.

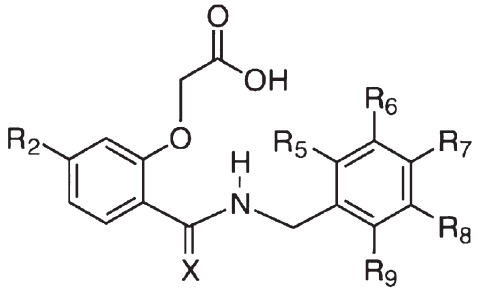

Figure 3. Scaffold for inhibitor preparation.

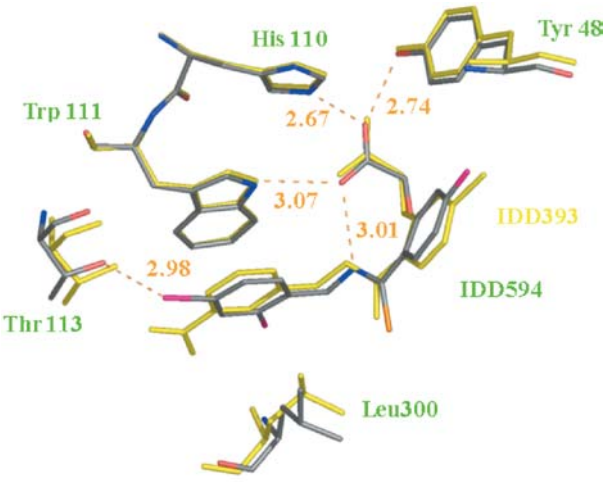

Figure 4. Superposition of carboxylate inhibitors IDD 393 (in yellow) and IDD 594, showing the contacts of IDD 594.

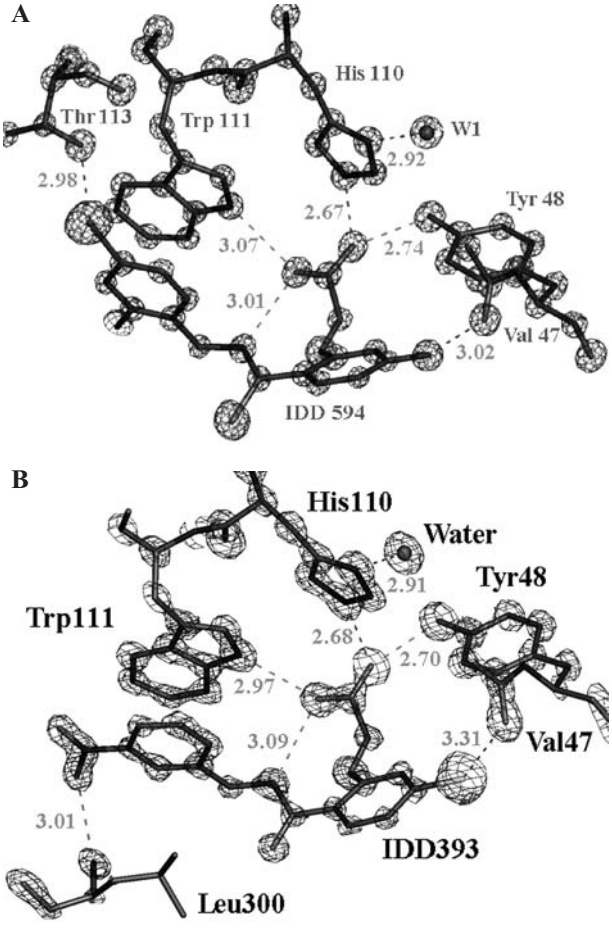

Figure 5 A, B. Electron density maps contoured at 2.5 σ around IDD594 (*a*, from [12]) and IDD 393 (*b*). Resolution: 0.66 Å and 0.9 Å, respectively. Ultra-high resolution allows differention of each atom from its neighbours. Electronic density peak sizes are proportional to the corresponding atomic number.

0.4 e/Å^2 (4.0 σ) (fig. 6) showed that His110 is singly protonated in the NE2 position, and that a water molec ule is the proton donor in the H bond with the ND1 atom. The difference between C-NE2 bond length (1.348 Å) and the C-ND1 bond length (1.330 Å) confirms the single protonation state of His110. This residue is H bonded with a carboxylate oxygen of the inhibitor.

The second carboxylate oxygen is a proton acceptor in the two H bonds, where it is involved [with NE1 of Trp111 (3.07 Å) and with the central nitrogen of IDD594 (3.01 Å)], because the two nitrogens are protonated for chemical reasons. The C-O bond lengths in the carboxylate group (1.243 and 1.266 Å) are consistent with a fully deprotonated state for this moiety (for a protonated carboxylate, the difference between the single and double bond lengths is at least 0.1 Å). One oxygen atom of the negatively charged carboxylate also interacts with the positively charged aromatic ring of the NADP$^+$ cofactor, at a distance of 3.06 Å from the nicotinamide C3 atom and at 3.17 Å from C4 (see fig. 7).

The most important hydrophobic interaction is observed in the specificity pocket: the stacking between one of the inhibitor rings and Trp111 (about 3.4 Å distance between planes), as shown in figure 8 for IDD 393.

The differences between IDD 594 and IDD 393 are found in the specificity pocket. While IDD 393 shows a hydrogen bond between the NO2 group and the main chain N atom of Leu 300 (fig. 8), IDD 594 shows an interaction between a polarised bromine and the oxygen of Thr 113 (fig. 9).

The stronger binding of IDD 393 shown by the IC50 values (30 nM for IDD594 vs. 6 nM for IDD393) indicates

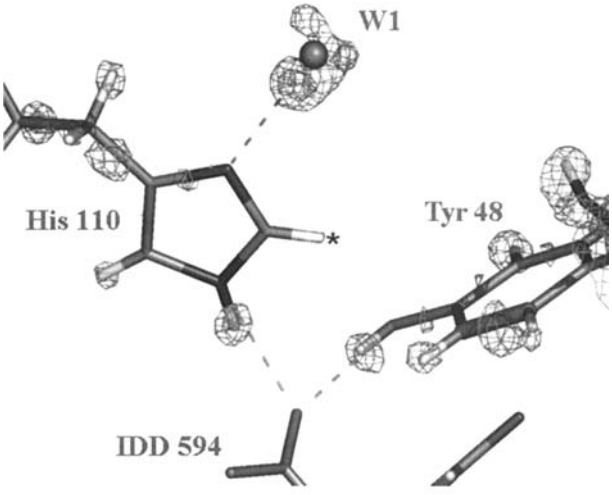

Figure 6. Difference map of the active site region with omited hydrogen atoms contoured 0.44 e/Å^3 (4.0 σ), in green at 0.31 e/Å^3 (2.8 σ from [25]). The single protonation of His110 is clearly visible. The strong peak [including a double contour at 0.44 e/Å^3 (4.0 σ) near the water molecule H bonded with the ND1 indicates that this molecule is the proton donor. Electronic densities in the bonds indicate deviations from the spherical atom model. The hydrogen atom linked to CE2, marked *, is visible at lower contours (0.11 e/Å^3).

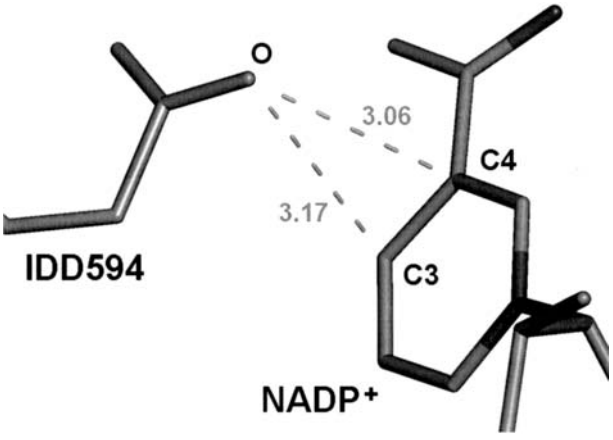

Figure 7. Interactions of the inhibitor IDD 594 carboxylate head.

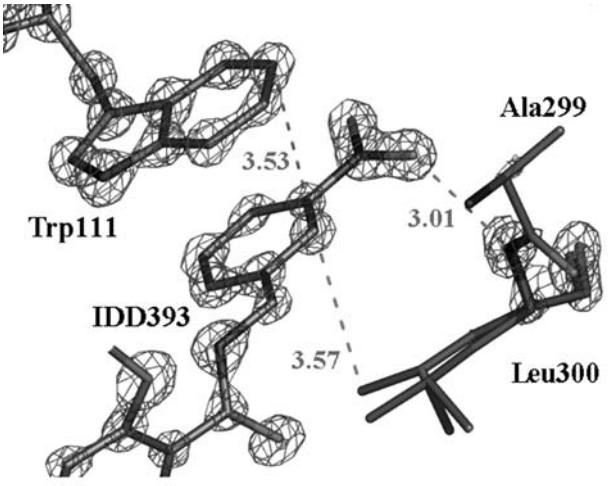

Figure 8. Stacking between one of rings of IDD393 and Trp111. Note also the interactions with Leu300.

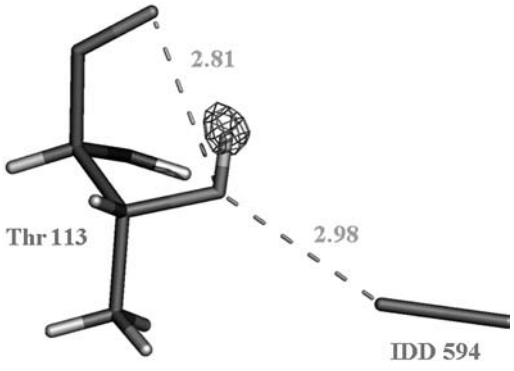

Figure 9. Interaction between a polarized bromine of IDD594 and the oxygen of Thr113 from [25]. Note the peak of the difference map (2.5 σ contour), showing that the side chain of the threonine makes an H bond with the main chain.

a stronger binding of IDD393. This might be due to a more favorable interaction in the specificity pocket, as shown by mass spectrometry measures of the electrostatic binding energy. This energy is estimated by the VC50 values, which indicates the voltage difference in a collision chamber necessary to dissociate half of the protein-inhibitor complex. The VC50 is 94 for IDD594 and 102 for IDD393. Therefore, the observed increase in binding of IDD393 vs. IDD594 is likely due to the electrostatic contribution of the NO2-N300 contact.

To confirm this hypothesis, free energy perturbation calculations [21] were performed in which IDD594 was gradually mutated into IDD393 and the difference in binding energies ΔΔG was calculated. The result is indicated in table 3, where $\Delta\Delta G_{IC50}$ is estimated from the IC50 differences and $\Delta\Delta G_{elect}$ is the electrostatic component of the free energy difference, mostly coming from the NO2-N300 interaction.

Comparison with other published carboxylate inhibitors

Inhibitor binding geometries similar to IDD 594 were observed with inhibitors statil [13] (fig. 10), tolrestat [19] (fig. 11) and zopolrestat [22] (fig. 12).

In all of these complexes the inhibitors have their carboxylate moieties firmly attached with His110, Tyr48 and Trp111 by H bonds and a ring – or a ring system – bound into the specifity pocket. Statil binds in a position very close to that of IDD594 [13]. The difference in the Br-OG113 distances (2.98 Å in IDD 594, 3.11 Å in statil) could be due to the different resolution of the crystallographic structure solution (0.66 Å for IDD 594, 2.1 Å for statil). The most significant divergence in this group is the perpendicular position into the specificity pocket of tolrestat [19].

A nonequivalent binding was found for IDD384 [23] crystallised at pH 5. This inhibitor – longer than the previous ones – binds without any substantial protein conformational change and without opening the specificity pocket (fig. 13).

The carboxylic group of these inhibitors shows a different position making H bonds with His110 and Tyr48 but none with Trp111. In contrast, a sulfonyl oxygen interacts with Trp111. The same inhibitor has another carboxyl conformation when complexed (at pH 6.2) with pig AR

Table 3. Differences in binding energies between IDD393 and IDD594.

$\langle\Delta\Delta G\rangle$ [kcal/Mol]	$\Delta\Delta G_{IC50}$ [kcal/Mol]	$\langle\Delta\Delta G_{elect}\rangle$ [kcal/Mol]
–2.5	–1.03	–2.0

Figure 10. Superpositon of the active site structures of the IDD594 complex (in yellow) and the statil complex. From [10]

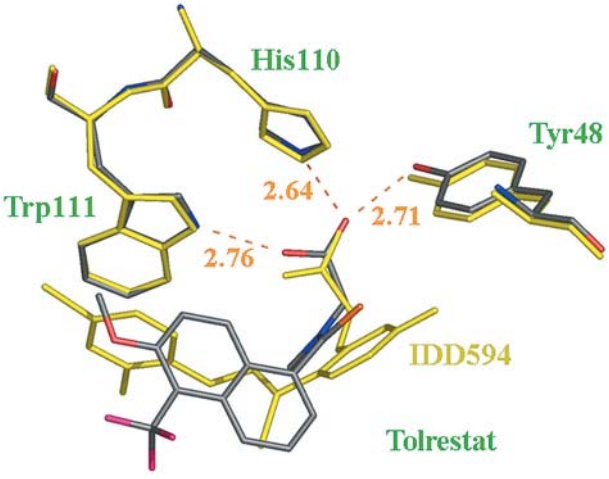

Figure 11. Superpositon of the active site structures of the IDD594 complex (in yellow) and the tolrestat complex [13].

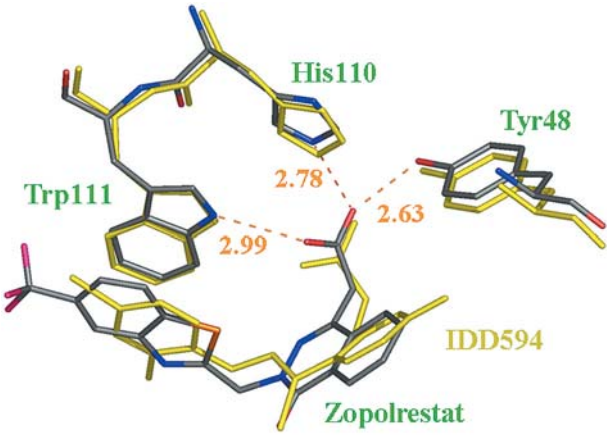

Figure 12. Superpositon of the active site structures of the IDD594 complex (in yellow) and the zopolrestat complex [14].

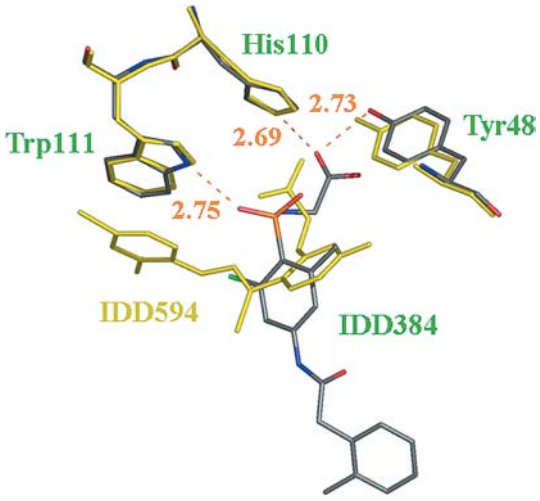

Figure 13. Superposition of the active site structures of the IDD594 complex (in yellow) and the IDD384 complex [15]. From Ref. [10].

[23]. As the pKa of IDD384 is 4.2, the inhibitor probably has a diferent protonation state in each complex (at pH 5 an important portion could be protonated). This difference highlights the correlation between the protonation state and the geometry of binding of the polar head of the inhibitor.

Cyclic imide inhibitors at subatomic resolution: SNK-860 and WAY-509

Within the same collaborative effort, two crystal structures were determined for the complexes with the bound inhibitors fidarestat (SNK-860) and minalrestat (WAY-509) [13] (fig. 14), both of them belonging to the cyclic imides group of AR inhibitors. The details of the solved structure are given in table 1. All atoms appear clearly in electron density maps, as shown in figure 15.

As shown in figure 16, carbonyl atoms of both inhibitors are H bonded with the Nε1 atom of Trp111(2.80 Å for fidarestat and 2.87 Å for minalrestat) and with the Tyr48 hydroxylate (2.63 Å and 2.60 Å, respectively). The nitrogen in the cyclic imide forms an H bond with His110 Nε1 in both cases (2.76 Å for fidarestat and 2.80 Å for minalrestat). The C-O bond distances in the cyclic imide rings (1.2 Å) indicate a double bond.

This observation supports the idea that inhibitors are negatively charged into the active site as has been observed by calorimetric assays in sorbinil, a member of the same family of AR inhibitors [O. Kraemer, personal communication].

The isoquinoline ring of minalrestat is placed into the specificity pocket stacked with Trp111 (mean distance of 3.65 Å). A bromine atom is placed at 3.02 Å from the

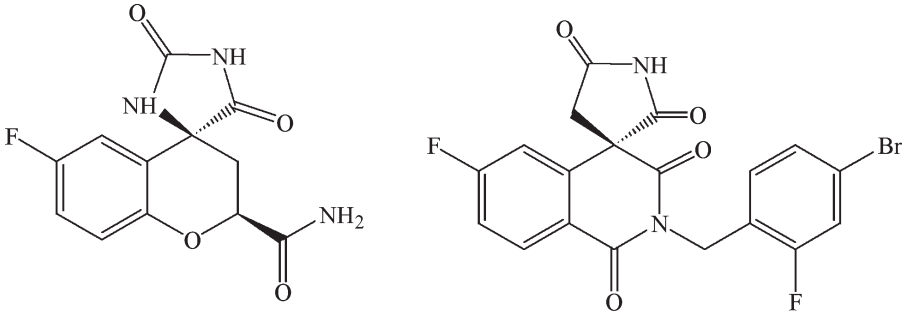

Figure 14. Scheme of fidarestat (left) and minalrestat (rigth) structures.

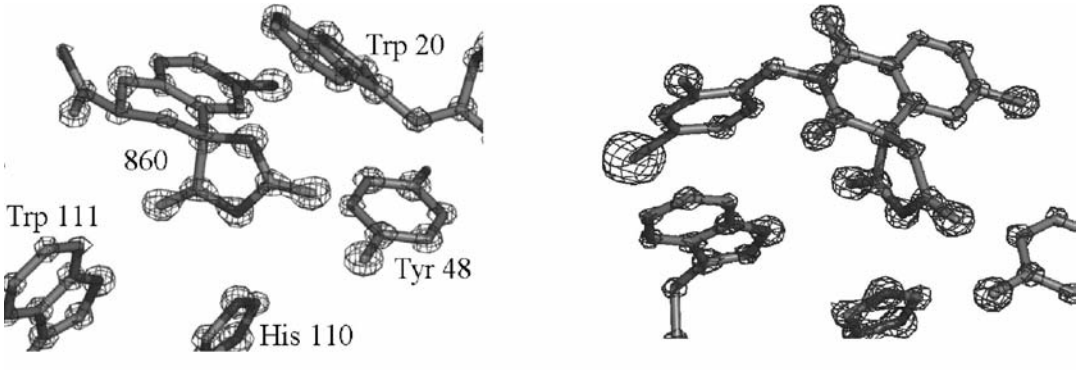

Figure 15. 2Fo-Fc σ-A weighted maps of fidarestat (right) and minalrestat (left) contoured at 4 σ from [25].

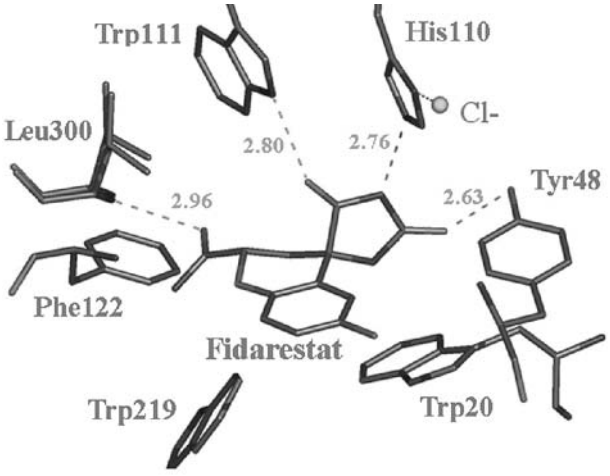

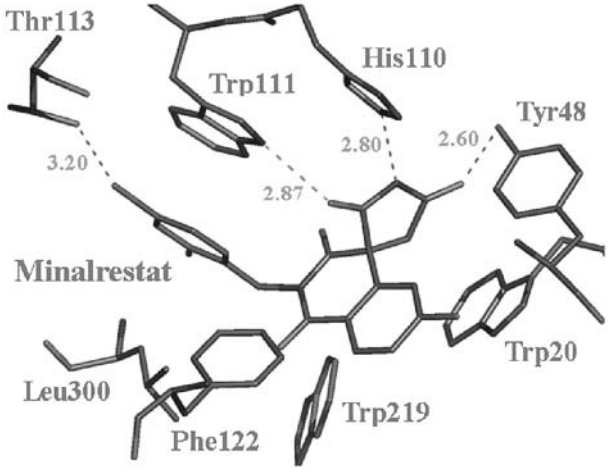

Figure 16. Contacts of fidarestat and minalrestat. For the case of fidarestat, note the chlorine ion interacting with His110 and the H-bond between the carboxyl oxygen of the inhibitor and N atom of Leu300.

OG1 of Thr113, a distance similar to that observed in the IDD594 complex. Fluorine atoms form H bonds with the main-chain nitrogen of Leu300 (3.20 Å; this distance is 0.1 Å longer in the IDD594 complex). The overall geometry is very close to IDD 594, as shown in figure 17.

In the fidarestat complex, the chroman ring has van der Waals contacts with residues: Trp20, Trp111, Phe122 and Trp219 (fig. 16). The oxygen atom of the carbonyl group forms an H bond with the N atom of the main chain of Leu300. In this complex this residue presents a double conformation (occupancies 63.6% and 36.4%) with H bond distances of 2.96 and 3.03 Å. Oka et al. [24] suggest that this interaction is the responsible of the high affinity of fidalrestat (a 1300 times more potent inhibitor against AR than against AR). The affinity of this residue is not due to the binding into the specificity pocket but to an H bond with one of the residues forming this region. In AR Leu300 is replaced by Pro, and the crucial H bond cannot be made.

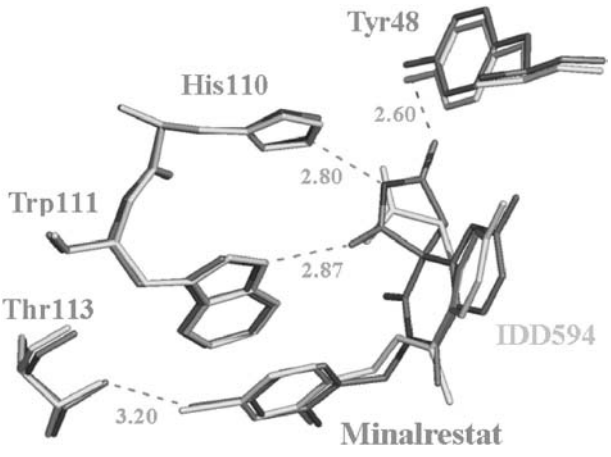

Figure 17. Superposition of minalrestat and IDD594.

Another feature was observed in this atomic resolution structure: the presence of a chlorine ion interacting with the Nε1 atom of His110 (3.06 Å) (fig. 18). Initially interpreted as a water molecule, the nature of the corresponding electronic density peak was unequivocally determined by means of anomalous scattering data.

The presence of the Cl^- ion can explain the binding of fidarestat in the neutral state, as proposed by the mechanism outlined in the scheme in figure 19. This scheme shows the following states:

I) In the native configuration, the active site is occupied by a citrate ion (observed in the native structure) which compensates the charge of $NADP^+$.

II) Part of the inhibitor binds in neutral state, displacing the citrate ion. Simultaneously, a Cl^- ion replaces the water molecule. This happens for fidarestat in ~80% of the cases (as indicated by the Cl^- occupation), and does not happen in minalrestat.

III) In fidarestat, the presence of the Cl^- ion positively shifts the pKa of His110, as indicated by theoretical

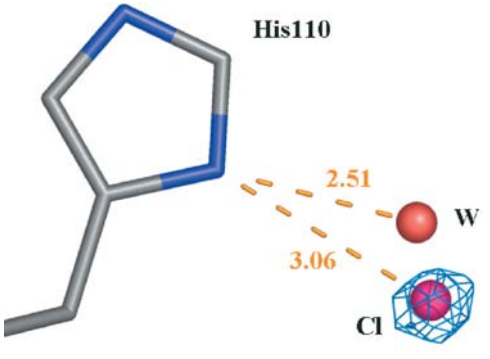

Figure 18. Anomalous difference map showing the peak corresponding to the Cl^- ion linked to His110 contoured at 6 σ. The water molecule represents an alternative molecule linked to the His110.

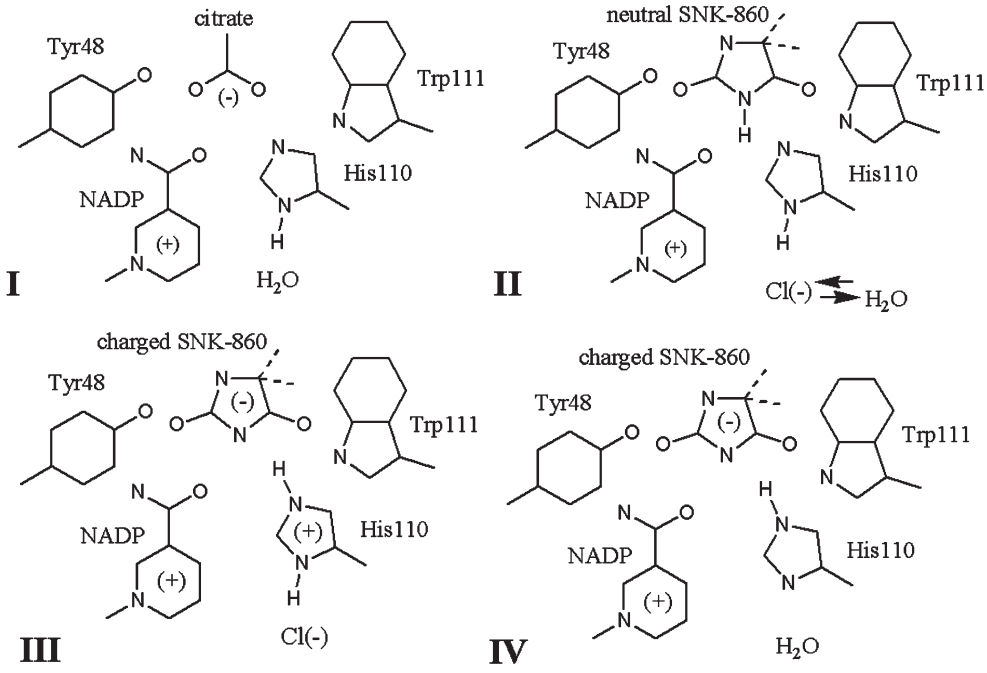

Figure 19. Scheme of fidarestat binding.

calculations [Ruiz et al. unpublished]. The histidine accepts the proton from the N1 atom of the hydantoin. An electrostatic interaction appears between the charged histidine and the charged inhibitor.

IV) Alternatively, a charged population of the inhibitor is bound in a way similar to that observed for the carboxylic acid inhibitors. In the fidarestat case, the occupation of the water molecule bound to His110 suggests that this happens in ~20% of the cases. With minalrestat, it happens for all cases.

The determination of His110 pKa as a function of Cl^- is necessary to elucidate the importance of this ion in the inhibitor-binding mechanism.

Considering as titrable the residues placed into the 10 Å sphere plus His41, His187 and His306, different theoretical states were analysed following the binding mechanism proposed by El-Kabbani et al. [13] (table 4). This mechanism starts with the $NADP^+$ bound to the protein after citrate leaving the active site and before inhibitor binding. In this state the pKa of His110 is very low (2.27), as was pointed out in previous work [19]. His110 is principally single protonated at pH 5. In the second step the neutral inhibitor binding reduces the pKa value of His110 still more (to 0.193). Single protonation is favored in the Nδ position, pointing to the water molecule (94.7 and 95.7% at pH 5 and 7.4, respectively). In the third step the water molecule is changed by the chlorine ion without changing the protonation state of the inhibitor. The pKa of His110 starts to rise but still is remarkably low (1.9). The protonation state is the same as in the previous step. Finally, the inhibitor lost a proton – becoming charged – and we see the crystallographic geometries.

The effect of chlorine ion is pointed out by the 3.854 units difference between the pKa values when the ion is considered (8.066) and when the water molecule is considered (4.212). When chlorine is placed near His110, this residue is principally double protonated (98.14 and 74.67% of probability at pH 5 and 7.4; respectively). When the water

Table 4. Comparison between the pKa values for His110 and Tyr48 when the atomic charges of charged molecules are zero. These results were obtained using the crystallographic structure and considering as titrable residues His41, Asp43, Cys44, His46, Tyr48, Glu51, Lys77, Cys80, His83, His110, His187, Tyr209, Cys298 and His306.

System	His110 pKa value	His110 ΔpKa	Tyr48 pKa value	Tyr48 ΔpKa
Chlorine ion with zero atomic charges	5.331	–1.6	9.004	1.1
$NADP^+$ with zero atomic charges	8.835	1.9	14.865	4.7
Fidarestat with zero atomic charges	4.091	–2.8	10.585	0.5
Chlorine ion, $NADP^+$ and fidarestat with zero atomic charges	1.592	–5.3	9.872	0.3

molecule is considered, His110 is mostly single protonated in the Nε atom. This protonation state is the observed one in the SNK509 [13], IDD393 and IDD594 [25] complex structures. In both cases a water molecule binds in this place, and no chlorine ion is observed.

The change in the pKa value of Tyr48 is 1.5 units (12.797 with chlorine, 11.261 with water). In both cases is protonated over the complete pH range of enzyme activity. Similar observations can be applied to Lys77, with pKa values of 21.22 and 20.21 when chlorine or water is considered, respectively.

The inhibitor effect was studied by deleting this molecule from the active site, which is considered to be full of water. The His110 pKa is reduced to 4.73. A similar value is found when a water molecule replaces, the ion, but in this case – without SNK860 – His110 is principally singly protonated in the Nδ atom, being a proton donor in an H bond with the ion.

Conclusions

The inhibition of AR is a field which has been widely studied, as reviewed in the previous article of this series. These studies include a number of crystallographic structures which help to explain the details of the mechanisms of catalysis and of inhibitors binding. These include the opening of the specificity pocket and occupation of the anionic hole in the active site cleft by the charged head of inhibitors. However, a number of questions remained open, such as the protonation state of active site residues and of the inhibitor, and the specific role of interactions in the specificity pocket, such as the ones implying the bromine atom. In some cases, such as the charge state of the bound head of the cyclic imides, these questions are puzzling, as the pKa of the inhibitor binding the anionic hole is too high to be charged in solution. Other techniques, such as microcalorimetry, mass spectrometry, site-directed mutagenesis and modelling, have been used to provide additional information, but the answers are necessarily indirect. Subatomic resolution crystallography has the major advantage of giving a direct image of the state of protonation of relevant residues; when coupled with anomalous scattering studies, it is also very powerful in resolving ambiguities about the atomic species. In the cases described, this introduces new information about binding, such as

1) Occupation and position of H atoms, for example those of His110 and Thr113, determine the strength binding interactions. This is complemented by the accurate measurement of bond lengths, interatomic distances, bond angles and torsion angles.
2) Determination of the precise distance of Br(inhibitor)-OG (Thr113), which implies a strong electrostatic interaction in the IDD594 complex.
3) Determination of the atomic species of the Cl^- ion bound to His110 is essential to determine the inhibitor binding mechanism, and in particular to explain how the hydantoin head can bind in the neutral state. The double conformation Cl^-/water suggests two modes of binding, neutral and charged.

This crystallographic information has provided the starting point for the precise calculation of binding energy differences using the free energy perturbation protocol and of the pKa's of the concerned residues. The results confirm the experimental information provided by the IC50 and VC50 (voltage at which half the complexes are associated in a mass spectrometry collision experiment) values. The ensemble provides an explanation of the mechanism of binding, which can then be used for drug design.

Acknowledgements. Special thanks to the SBC and SLS staff for their support in data collection, and the IGBMC and NCI staff for computer assistance and useful discussions, Dino Moras for support and F. Ruiz for his help with figure preparation. This work was supported by the Centre National de la Recherche Scientifique (CNRS), by collaborative projects CNRS-CONICET, CNRS-CERC and CNRS-NSF (INT-9815595), by Ecos Sud, by funds from the U.S. National Cancer Institute (contract no. NO1-CO-12400) and the National Institutes of Health, by the Institut National de la Santé et de la Recherche Médicale and the Hôpital Universitaire de Strasbourg (H.U.S), and by the Institute for Diabetes Discovery, Inc., through a contract with CNRS, and in part by the U.S. Department of Energy, Office of Biological and Environmental Research, under contract no. W-31-109-ENG-38. The content of this publication does not necessarily reflect the views or policies of the Department of Health and Human Services, nor does mention of trade names, commercial products or organisations imply endorsement by the U.S. Government.

1 Giacovazzo C., Monaco H., Viterbo D., Scordari F., Gilli G., Zanotti G. et al. (1992) Fundamentals of Crystallography. Oxford Univertiy Press, Oxford
2 Heinemann U., Illing G. and Oschkinat H. (2001) High-throughput three-dimensional protein structure determination. Curr. Opin. Biotechnol. **12:** 348–354
3 Schulz W. G. (2001) Determining Structure. Chem. Eng. News **79:** 23–26
4 Teeter M. M., Roe S. M. and Heo N. H. (1993) Atomic resolution (0.83 A) crystal structure of the hydrophobic protein crambin at 130 K. J. Mol. Biol. **230:** 292–311
5 Jelsch C., Teeter M. M., Lamzin V., Pichon-Pesme V., Blessing R. H. and Lecomte C. (2000) Accurate protein crystallography at ultra-high resolution: valence electron distribution in crambin. Proc. Natl. Acad. Sci. USA **97:** 3171–3176.
6 Kuhn P., Knapp M., Soltis M., Ganshaw G., Thoene M. and Bott R. (1998) The 0.78 Å Structure of a serine protease: *Bacillus lentus* subtilisin. Biochemistry **37:** 13446–13452
7 Howard E., Lamour V., Mitschler A., Barth P., Moras D. and Podjarny A. (1999) Resolution improvement to 0.9A in crystals of human aldose reductase. Acta Cryst. **A55 Suppl.** P09.OB.001
8 Dauter Z., Lamzin V. S. and Wilson K. S. (1997) The benefits of atomic resolution. Curr. Opin. Struct. Biol. **7:** 681–688.
9 Esposito L., Vitagliano L. and Mazzarella L. (2002) Recent advances in atomic resolution protein crystallography. Protein Peptide Lett. **9:** 95–105

10 Schmidt A. and Lamzin V. S. (2002) Veni, vidi, vici – atomic resolution unraveling the mysteries of protein function. Curr. Opin. Struct. Biol. **12:** 698–703
11 Cachau R., Howard E., Barth P., Mitschler A., Chevrier B., Lamour V. et al. (2000) The subatomic resolution structure of human aldose reductase shows the catalytic mechanism. Journal de Physique **10:** 3–13
12 El-Kabbani O., Darmanin C., Schneider T. R., Hazemann I., Ruiz F., Oka M. et al. (2003) Ultra-high resolution drug design II: atomic resolution structures of human aldose reductase holoenzyme complexed with fidarestat and minalrestat; implications for the binding of cyclic imide inhibitors. Proteins Struct. Funct. Genet. In press
13 El-Kabbani O., Ramsland P., Darmanin C., Chung R. P. T. and Podjarny A. (2003) Structure of human aldose reductase holoenzyme in complex with statil: An approach to structure-based inhibitor design of the enzyme. Proteins Struct. Funct. Genet. **50:** 230–238
14 Lamour V., Barth P., Rogniaux H., Poterszman A., Howard E., Mitschler A. et al. (1999) Production of crystals of human aldose reductase with very high resolution diffraction. Acta Crystallogr. D **D55:** 721–723.
15 Rossmann M. Ed. (1972) The molecular Replacement method. A Collection of papers on the Use of Non-Crystallographic Symmetry. Gordon and Breach, New York
16. Navaza J. (1994) Amore – an automated package for molecular replacement. Acta Cryst. Section A **50:** 157–163
17 Miyamoto S. (2002). Recent advances in aldose reductase inhibitors: potential agents for the treatment of diabetic complications. Expert. Opin. Ther. Patents **12:** 621–631
18 Oates P. J. and Mylari B. L. (1999) Aldose reductase inhibitors: therapeutic implications for diabetic complications. Expert Opin Investig Drugs **8:** 2095–2119
19 Urzhumtsev A., Tete-Favier F., Mitschler A., Barbanton J., Barth P., Urzhumtseva L. et al. (1997) A 'specificity' pocket inferred from the crystal structures of the complexes of aldose reductase with the pharmaceutically important inhibitors tolrestat and sorbinil. Structure **5:** 601–612
20 Rick S. W. and Cachau R. E. (2000) The nonplanarity of the peptide group: molecular dynamics simulations with a polarizable two-state model for the peptide bond. J. Chem. Phys. **112:** 5230–5241
21 McCammon J. A. (1991) Free energy from simulations. Curr. Opin. Struct. Biol. **1:** 196–200
22 Wilson D. K., Tarle I., Petrash J. M. and Quiocho F. A. (1993) Refined 1.8 A structure of human aldose reductase complexed with the potent inhibitor zopolrestat. Proc. Natl. Acad. Sci. USA **90:** 9847–9851
23 Calderone V., Chevrier B., Van Zandt M., Lamour V., Howard E., Poterszman A. et al. (2000) The structure of human aldose reductase bound to the inhibitor IDD384. Acta Crystallogr. D **D56:** 536–540
24 Oka M., Matsumoto Y., Sugiyama S., Tsuruta N. and Matsushima M. (2000) A potent aldose reductase inhibitor, (2S,4S)-6-fluoro-2′,5′-dioxospiro chroman-4,4′-imidazolidine -2-carboxamide (Fidarestat): its absolute configuration and interactions with the aldose reductase by X-ray crystallography. J. Med. Chem. **43:** 2479–2483.
25 Howard E., Sanishvili R., Cachau R., Mitschler A., Chevrier B., Barth P. et al. (2003) Ultra-high resolution drug design I: details of interactions in human aldose reductase-inhibitor complex at 0.66 Å. Prot. Struct. Funct. Genet., in press
26 Podjarny A., Schneider T. R., Cachau R. E., Joachimiak A. (2003) Structural information content at high resolution: MAD versus native. Methods Enzymol. **374:** 321–341